Applied Energy 121 (2014) 20–27

Contents lists available at ScienceDirect

Applied Energy

journal homepage: www.elsevier.com/locate/apenergy

A new neural network model for the state-of-charge estimation in the battery degradation process

LiuWang Kang *, Xuan Zhao, Jian Ma

Vehicle Engineering, Chang'an University, Xi'an 710064, PR China

HIGHLIGHTS

- Predict practicable capacity by cycle life model in the battery degradation process.
- Build a new RBFNN model based on cycle life model to estimate the SOC.
- Evaluate the robustness of new model against varying aging levels and temperatures.
- Assess the robustness of new model against varying loading profiles.
- Analyze the measurement of the battery aging cycles in electric vehicles.

ARTICLE INFO

Article history:
Received 18 June 2013
Received in revised form 5 January 2014
Accepted 25 January 2014
Available online 21 February 2014

Keywords:
State-of-charge
Electric vehicle
Cycle life model
Neural network
Robustness analysis

ABSTRACT

Battery state-of-charge (SOC) is a key parameter of the battery management system in the electric vehicle. To predict the practicable capacity of the battery in the degradation process, the cycle life model is built based on the aging cycle tests of the 6Ah Lithium Ion battery. Combined with the cycle life model, a new Radial Basis Function Neural Network (RBFNN) model is proposed to eliminate the battery degradation's effect on the SOC estimation accuracy of the original trained model. This proposed model is verified through the 6Ah Lithium Ion battery. First, Urban Dynamometer Driving Schedule (UDDS) and Economic Commission of Europe (ECE) cycles are experimented on the batteries under different temperatures and aging levels. Then, the robustness of the new RBFNN model against different aging levels, temperatures and loading profiles is tested with the datasets of the experiments and compared against the conventional neural network model. The simulations show that the new model can improve the accuracy of the SOC estimation effectively and has a good robustness against varying aging cycles, temperatures and loading profiles. Finally, the measurement of actual aging cycles of the battery in electric vehicles is discussed for the SOC estimation.

1. Introduction

As the key parameter of the battery management system, state-of-charge (SOC) can indicate the remaining energy of the battery directly [1]. The accurate SOC estimation is vital for the battery management system to predict the remaining range. Furthermore, it also helps to determine an effective management strategy which can avoid over-charging and over-discharging.

In recent years, the main methods for the SOC estimation include the current integral method [2,3], the open-circuit voltage method [4–6], the equivalent circuit method [7,8], the electrochemical model-based method [9,10], the Kalman filter method [2,11], the extended Kalman filter method [12–16] and artificial neural network models [17–24]. The current integral method is easy to implement, but it may result in the accumulated SOC estimation error. For the open-circuit voltage method, the open-circuit voltage should be measured only after the battery stops some time later, but the running electric vehicle cannot be in the quiescence for a long time. Based on the empirical equation, the equivalent circuit model cannot reflect the dynamic behavior of the battery well because the parameters are generally obtained from the steady state. The electrochemical model-based method may have too complicated mathematical structure to operate or would have to sacrifice its ability of capturing dynamic behavior to achieve a simple structure [9]. The Kalman filter method is a linear filter, but the battery model is nonlinear, so it is easy to generate big estimation error. The extended Kalman filter method is

* Corresponding author. Address: Vehicle engineering, Chang'an University, Middle Erhuan Road, Xi'an 710064, PR China. Tel.: +86 13488323464; fax: +86 02982334458.
E-mail address: liuwangkang@hotmail.com (L. Kang).

http://dx.doi.org/10.1016/j.apenergy.2014.01.066
0306-2619/

sensitive to system parameters and will give unreliable estimation if the nonlinearities of the battery model are severe [16]. As a very nonlinear black box system, the conventional artificial neural network model (CM) does not need accurate formulas to describe the relationship between the battery parameters and the SOC because the relationship can automatically be generated when training the network with the history data (current, voltage and temperature) [23,24]. However, the practicable capacity of the battery will decline when the battery has been used for many times or the temperature becomes severe. The earlier network which is trained based on the history data cannot eliminate the negative effect of the battery degradation on the SOC estimation. To solve the problem, CM should retrain the network with the updated training data [19]. However, the degradation of the battery changes constantly and its process is very complicated, which will bring about several issues including when and how often to retrain the network.

To overcome above defect of CM, the paper proposes a new RBFNN model to estimate the SOC. In this approach, the cycle life model is built to predict the practical capacity based on the aging cycle tests of the 6Ah Lithium Ion battery at different temperatures. As an input parameter of the proposed new model (PM), the predicted capacity of the battery would change in response to the varying temperatures and aging levels, which makes PM suitable for the SOC estimation of the battery in the degradation process.

The paper is organized as follows: in Section 2, the paper carries out the aging cycle tests of the 6Ah Lithium Ion battery at different temperatures and builds the cycle life model to predict the practicable capacity of the battery in the degradation process. In Section 3, Based on the cycle life model, a new RBFNN model is designed for SOC estimation. Meanwhile, the rules of adjusting network parameters are applied to modify network parameters and adjust the network structure with the training data samples. In Section 4, UDDS and ECE datasets of low aging-level battery at different temperatures are collected to train the new model in the variable power discharging experiments, and then the trained network is tested by UDDS and ECE datasets of the battery under different aging levels and temperatures. The estimating performance of PM is evaluated and compared with CM. Finally, the measurement equation is proposed to determine the actual aging cycles of the battery in electric vehicles with the running mileage of the battery.

2. The new model using RBFNN

2.1. The cycle life model of the Lithium Ion battery

The Lithium Ion battery always degrades with the time in real operations. And the degradation can be manifested as the capacity loss. The capacity loss is partly due to the loss of the recyclable Li-ions caused by many factors, such as cathode structure degradation, side reactions, passivation form and lithium plating at the anode [25]. The above factors change greatly under different temperatures and aging levels of the battery [26]. So it is significant for the battery management system to study the effect of the temperature and aging level on the capacity loss, which equals the difference between the nominal capacity and the practical capacity.

According to the battery test specification of national 863 high technology projects [27], the aging cycle test of the battery is a process which consists of the constant current charge, constant voltage charge and constant current discharge. In the paper, the aging cycle test of the 6Ah Lithium Ion battery (the selected battery was 6Ah LiMn2O4 type, which was developed by WESTECH INDUSTRY&TRADING CO., LIMITED) is accomplished respectively at 10 °C, 25 °C and 40 °C. The process of the aging cycle test is showed in Fig. 1. During the whole process, the practicable capacity of the battery is measured every 25 aging cycles. One aging cycle is showed in Fig. 2.

The results of the aging cycle tests at different temperatures are showed in Fig. 3. As the age cycles of the battery increase, the cell polarization will exist in the Lithium Ion battery and the amount of recyclable Li-ions in the anode will become less, which could cause capacity fade. As for the phenomenon that the practical capacity of

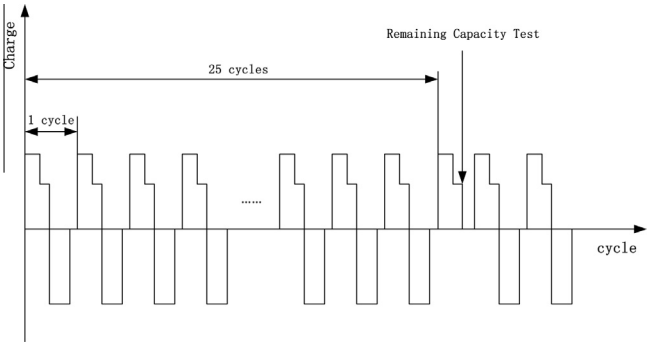

Fig. 1. The aging cycle test of the 6Ah Lithium Ion battery.

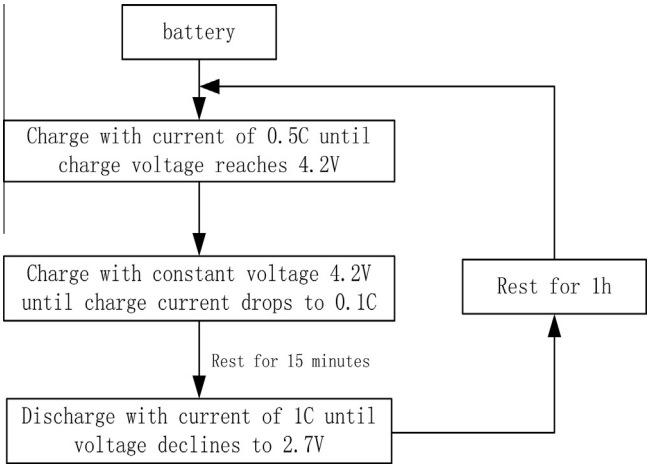

Fig. 2. The schedule of one aging cycle.

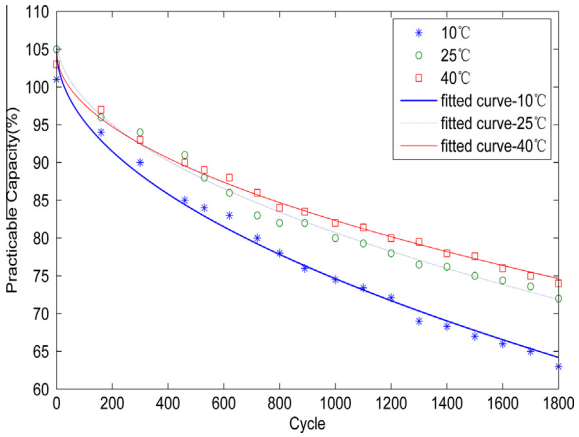

Fig. 3. Practicable capacity of the 6Ah Lithium Ion battery in the degradation process.

the battery at 10 °C has the sharpest decline while that of the battery at 40 °C shows the slowest degradation, it is mainly because that the electrode materials and the structure of the battery are easy to suffer some irreversible changes at low temperature. Moreover, the electrolyte of Lithium Ion battery is organic electrolyte and its conductivity will drop rapidly at low temperature [28]. So the impedance of the battery at low temperature will increase dramatically compared with that of the battery at relevant high temperature, which may explain why the practical capacity of the battery at 10 °C declines most dramatically and that of battery at 40 °C falls slowest.

As showed in Fig. 3, the practicable capacity of the battery has the remarkable regularity related to the aging level [29], so the mathematical relationship between the practicable capacity and aging cycles can be fitted as:

$$C_n = ax^{0.5} + b \tag{1}$$

where C_n is the practicable capacity of the battery; x is the aging cycles of the battery; a and b are the constants obtained by the data fitting. The fitting values of the constants at different temperatures are showed in Table 1. The expression reflects the tendency of the practicable capacity varying with the temperatures and the aging cycles.

To ensure that the cycle life model can predict the practicable capacity of the battery in the degradation process exactly, a new feedback can be formed to correct the cycle life model. The actual capacity of the battery can be measured every 20 aging cycles in practical application and compared with the predicted capacity. The age cycles of the battery will be adjusted to correct the predicted capacity if any two consecutive estimated errors of the capacity are both above 3%.

2.2. The structure of the RBFNN

Shown in Fig. 4, the RBFNN is consisted of 3 layers-the input layer, the hidden layer and the output layer. In the input layer, the input parameters are instantaneous terminal voltage, current and practicable capacity. To realize the nonlinear transformation from the input layer to the hidden layer, a series of the Radial Basis Functions constitute the hidden layer. As the terminal port of the model, the output layer is the estimated SOC.

Table 1
The constants of the cycle life model of the 6Ah Lithium Ion battery.

Parameter	Mean value	Confidence (95%) internal
a	−0.009638 (T = 10 °C)	[−0.010480, −0.008793]
	−0.008185 (T = 25 °C)	[−0.008687, −0.007682]
	−0.007107 (T = 40 °C)	[−0.007436, −0.006778]
b	1.051 (T = 10 °C)	[1.025, 1.077]
	1.066 (T = 25 °C)	[1.051, 1.082]
	1.048 (T = 40 °C)	[1.038, 1.058]

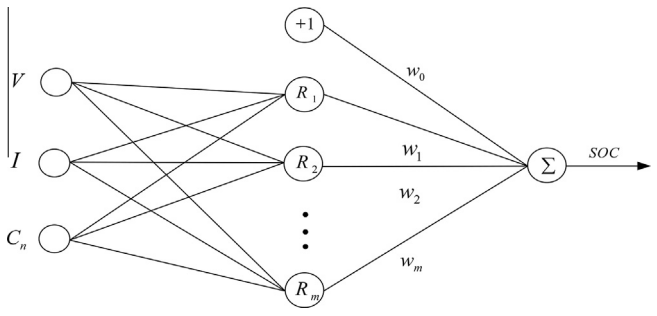

Fig. 4. The new structure of RBFNN for SOC estimation.

In the hidden layer, the Radial Basis Function only responses to the input layer signal in partial region and will give the maximum response when the input signal is in the center of the partial region. The Gaussian Function in the paper is given as follows:

$$R_i(x_p) = G(\|x_p - t_i\|) = \exp[-\|x_p - t_i\|^2/\sigma_i^2] \quad i = 1, 2, \cdots, m \tag{2}$$

where i is the sequence number of the Gaussian Functions in the hidden layer; m is the total number of the Gaussian Functions in the hidden layer; x_p=$[V\ I\ C_n]^T$ is the input vector of the pth training data sample; t_i, the center of the ith Gaussian Function, means the location of the ith Gaussian Function; σ_i, the standard deviation of the ith Gaussian Function, shows the width of the ith Gaussian Function; $\|x_p - t_i\|$, the vector norm, describes the Euclidean distance between the input vector of the pth training data sample and the center of the ith Gaussian Function.

Fig. 4 shows that the output layer maps the Gaussian Function outputs linearly. In the RBFNN, the activity function of the output layer is a summing work, so the estimated SOC is the summation of the weighted Gaussian Function outputs. When the input vector of the model is x_p, the estimated SOC can be expressed as:

$$SOC_e(p) = w_0 + \sum_{i=1}^{m} w_i \cdot R_i(x_p) \tag{3}$$

where w_i is the weighted value of the Gaussian Function output.

3. SOC estimation based on the RBFNN

When the new RBFNN model estimates SOC for the first time, a number of data samples $[V\ I\ C_n\ SOC_a]$ are selected to train the model primarily. Based on the defined objective error function, the model will keep adjusting Gaussian Function centers, standard deviations and weighted values until all the training data samples participate in training.

In the paper, the defined objective error function ε is:

$$\begin{aligned}\varepsilon(k) &= \frac{1}{2}\sum_{p=1}^{k}(SOC_a(p) - SOC_e(p))^2 \\ &= \frac{1}{2}\sum_{p=1}^{k}\left(SOC_a(p) - w_0 - \sum_{i=1}^{m} w_i \cdot R_i(x_p)\right)^2\end{aligned} \tag{4}$$

where $\varepsilon(k)$ is half the sum of square errors between the estimated SOC and the actual SOC when the number of the training data samples equals k; $SOC_a(p)$ is the corresponding actual SOC of the pth training data sample and $SOC_e(p)$ is the corresponding estimated SOC of the pth training data sample.

The rules of adjusting network parameters in the paper will be described as follows:

The network parameter is defined to be V_p after trained with the pth training data sample. When trained with the p + 1th training data sample, the network parameter V_{p+1} will be modified as:

$$V_{p+1} = V_p + \alpha \cdot \Delta V = V_p + \alpha\frac{\partial \varepsilon}{\partial V} \tag{5}$$

where $V = [t\ \ \sigma\ \ w]$, t is the Gaussian Function center; σ is the standard deviation; w is the weighted value and α is the learning efficiency.

4. Experiments and simulations

4.1. Acquire data samples

In order to collect UDDS and ECE datasets to train and test the new model, we did variable power discharging experiments with the 6Ah Lithium Ion battery on the battery platform. The battery

platform is consisted of programmable electronic load module, data acquisition module, charge and discharge module and safety-protection module. The above experiments are executed severally at 10 °C, 25 °C and 40 °C. As showed in Fig. 5, the experiment includes the aging cycle test and driving operation test (UDDS and ECE). To evaluate the model's robustness against different aging levels, the battery will suffer the operation test when the aging cycles are 50, 100,400 and 700 respectively. The UDDS and ECE datasets of the battery (50 aging cycles) at 10 °C, 25 °C and 40 °C are used to train the model, while the datasets of other aging cycles are applied to test the performance of the trained model. The details of variable power discharging experiment in the paper are in this order:

First, through the software ASVISOR (Advanced Vehicle Simulator), we can obtain the power values demanded by the electric vehicle which runs respectively at UDDS operation and ECE operation. And then scale these power values down to the range of the 6Ah Lithium Ion battery power values.

Second, utilize the programmable electronic load module to set the discharging process for the full-charge Lithium Ion battery and to simulate the sequence of the contractible power values. At the same time, set the battery cut-off voltage to avoid over-discharging.

Third, set the sampling rate of the data acquisition module to be 1HZ and start the data acquisition module to collect instantaneous terminal voltage and current automatically. The current is measured by WT1600 power analyzer, WT1600 has the measurement range from 10 mA to 50A and its current measurement accuracy is ±0.1%. Stop the discharging process and then save the data when the battery reaches the battery cut-off voltage.

Finally, based on the temperature and the aging cycles of the battery, calculate the practicable capacity C_n for the cycle life model of the battery.

In the paper the current integral method is applied to estimate SOC. The actual SOC would be calculated after Lithium Ion battery has suffered the operation test. The total practical capacity could be obtained by integrating the current curve of the whole process, which avoids the problem of the total practical capacity estimation.

4.2. Model simulation

Huge differences exist in the value ranges of the original dataset. The rectifications of network parameters would be affected seriously during the training process if training data samples sent to the RBFNN were directly selected from the original data. Normalizing the original data can eliminate that negative influence and is also apt to improve the convergence rate of the training. The post-processing data after the normalization in the paper ranges from −1 to 1.

Training data samples are selected randomly from the whole post-processing UDDS and ECE datasets of the batteries (50 aging cycles) at 10 °C, 25 °C and 40 °C. After trained by the training data samples, PM and CM will be tested by post-processing UDDS and ECE datasets of the batteries (100, 400 and 700 aging cycles) at 10 °C, 25 °C and 40 °C. Finally, the estimated results of PM and CM are contrasted and evaluated.

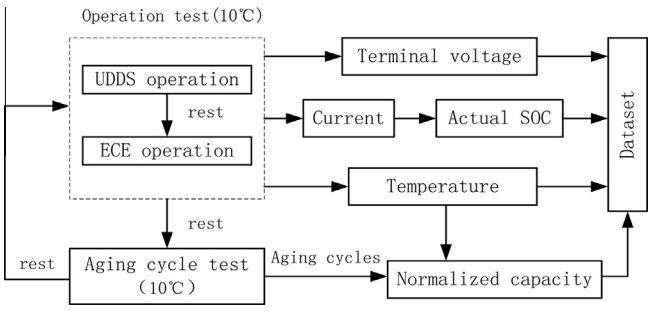

Fig. 5. The operation test at 10 °C to collect dataset.

5. Results and discussions

5.1. The robustness of PM against different temperatures and aging levels

UDDS datasets under different temperatures and aging levels are collected to evaluate the robustness of the PM. Its performance is compared with the CM.

Fig. 6a shows the discharging current profile of the battery (50 aging cycles) under UDDS operation at 25 °C. According to Section 4.1, the actual SOC profiles of the battery (50 and 100 aging cycles) are calculated and showed in Fig. 6b. Based on the cycle life model, the practical capacity (relative to the nominal capacity) at 25 °C is 1.0081 for the selected Lithium-ion battery of 50 age cycles and the practical capacity at 100 age cycles is 0.9842, indicating that the capacity loss increases very slowly during this period. The actual SOC curves of the battery at 50 age cycles and 100 age cycles in Fig. 6b are nearly identical, which may indirectly verify the cycle life model.

Further, Fig. 6b also includes the comparison of the estimated SOC curves between PM and CM when the battery has 100 age cycles. The corresponding SOC estimation errors for the PM and CM are showed in Fig. 7a. The mean absolute error (MAE) for PM is 2.4% while the MAE for CM is 3.4%. This reflects that PM can

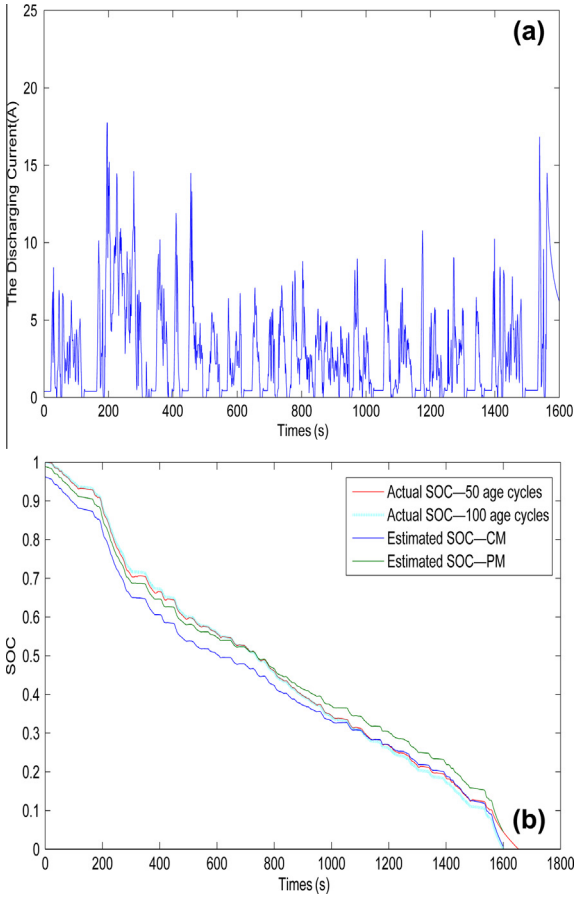

Fig. 6. UDDS dataset of the battery at 25 °C: (a) the discharging current profile (50 aging cycles); (b) actual SOC profiles and estimated SOC profiles.

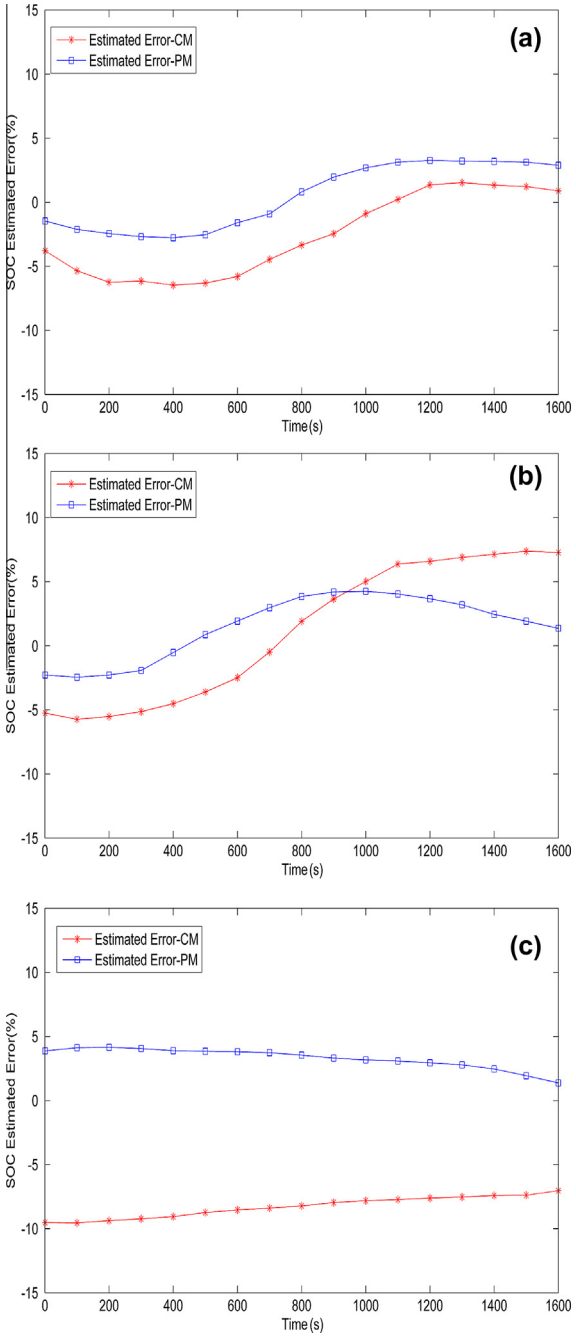

Fig. 7. SOC estimation error of the battery at 25 °C (UDDS operation): (a) 100 aging cycles; (b) 400 aging cycles; (c) 700 aging cycles.

decrease the SOC estimation error more efficiently compared with CM.

When the temperature is 25 °C, the SOC estimation errors and the MAE under different aging levels for PM and CM are showed in Figs. 7 and 8 respectively. It can be seen that PM compensates for the gradation of the battery efficiently and has a better accuracy than CM, it is mainly because that the cycle life model of the battery provides relatively accurate practicable capacity for PM. The practicable capacity of the Lithium Ion battery will reduce about 10% when the battery is 400 aging cycles. When the aging cycle is 700, it will reduce about 15% which is near to the end of the typical life expectancy accepted for automotive applications. As showed in Fig. 8, the degradation of the battery has a less negative impact on the PM than on CM. the SOC estimation result of PM and CM at 10 °C and 40 °C are similar.

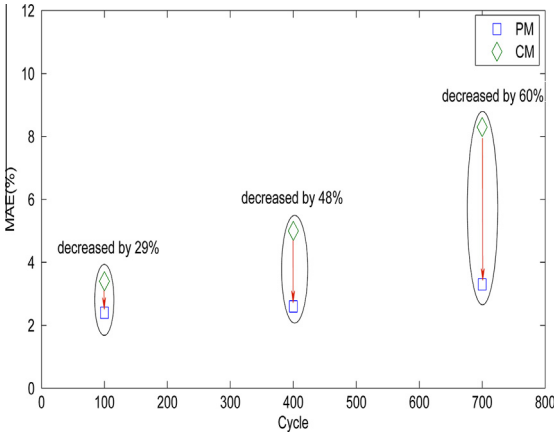

Fig. 8. The MAE of SOC estimation for PM and CM at 25 °C (UDDS operation).

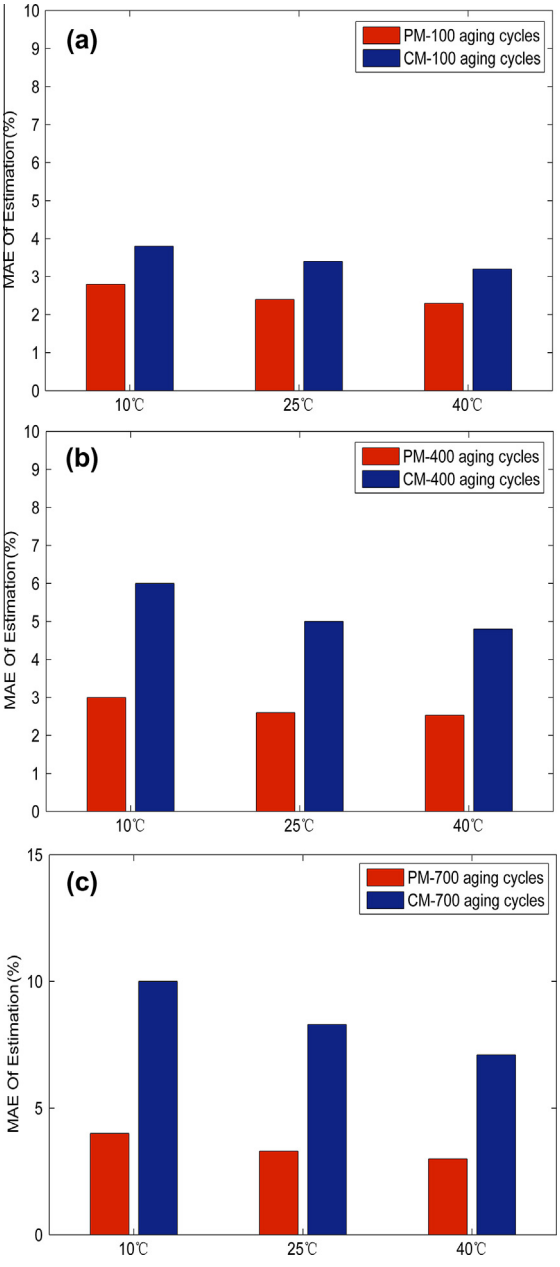

Fig. 9. The MAE of SOC estimation for PM and CM at three different temperatures (UDDS operation): (a) 100 aging cycles; (b) 400 aging cycles; (c) 700 aging cycles.

To compare the overall performance of PM with CM more clearly, the MAE under different temperatures and aging cycles are showed in Fig. 9. For the battery under three different age cycles, The differences of the MAE from 25 °C to 10 °C is average of 1.03% for CM while that for PM is 0.5%. Meanwhile, The differences of the MAE from 25 °C to 40 °C is average of 0.53% for CM while that for PM is 0.16%. It's obvious that PM has a better robustness against different temperatures than CM. For CM and PM, the mean difference values of MAE from 25 °C to 10 °C are both greater than that from 25 °C to 40 °C, because the practicable capacity of the Lithium Ion battery reduces significantly and its dynamic behavior changes noticeably from 25 °C to 10 °C. As showed in Fig. 9, the MAE of estimation under different temperatures and aging cycles for PM is all below 5%, indicating that PM has an accurate estimation of SOC and a good robustness against varying temperatures and the degradation of the battery.

5.2. The robust against different loading profiles

The battery always experiences many different working operations before the end of its life. So it is necessary to compare the robust against different loading profiles between PM and CM. The condition at ECE operation for the battery is very different from that under UDDS operation, PM and CM are also applied to estimate the SOC of the battery under ECE operation. Fig. 10a describes the discharging current profile of the Lithium Ion battery (50 aging cycles at 25 °C) under ECE operation. Since the current profile becomes less random and more stable than that under UDDS, the SOC under ECE operation changes more gently. Fig. 10b shows the SOC estimation comparison between CM and PM when the Lithium Ion battery has suffered 400 aging cycles. As the state-of-the-art method in this field, Extended Kalam Filter (EKF) is also applied to verify the estimation performance of PM. the result shows that the average estimation error between actual SOC and estimated SOC for CM is 4.6% and that for PM is 2.1%-an improvement by 54%. The average estimation error for EKF could reach only 1.1%, reflecting that EKF has higher estimation accuracy compared with the neural network method. However, an accurate SOC estimation based on EKF requires accurate model parameters and system parameters, which limits EKF's wide application.

The comparison of the MAE (400 aging cycles) between UDDS operation and ECE operation for PM and CM is showed in Fig. 11. It can be seen that under three different temperatures the MAE of estimation at ECE operation for PM and CM all drop down. The minimum MAE under ECE operation for CM is above 4%. While the maximum MAE under ECE operation for PM reduces to 3%, indicating that PM has a better robustness against different loading profiles than CM.

5.3. The measurement of the aging cycles in electric vehicles

When PM is applied to estimate SOC in practical application, the aging cycles of the battery in electric vehicles will be not easy to achieve. So it is necessary to calculate the aging cycles indirectly with other easy-measured parameters. For the battery in electric vehicles, the practicable capacity can be determined by the history

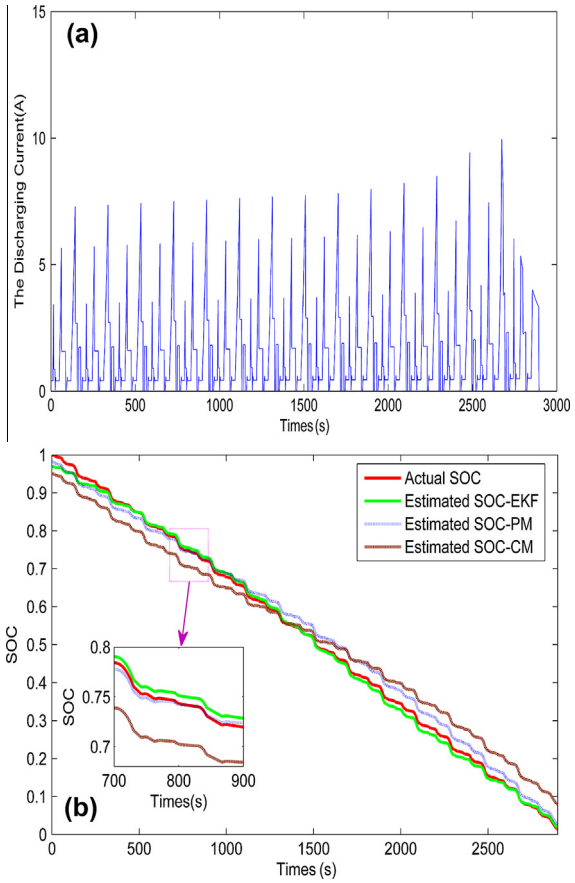

Fig. 10. ECE dataset of the battery at 25 °C: (a) the discharging current profile (50 aging cycles); (b) SOC profiles comparison.

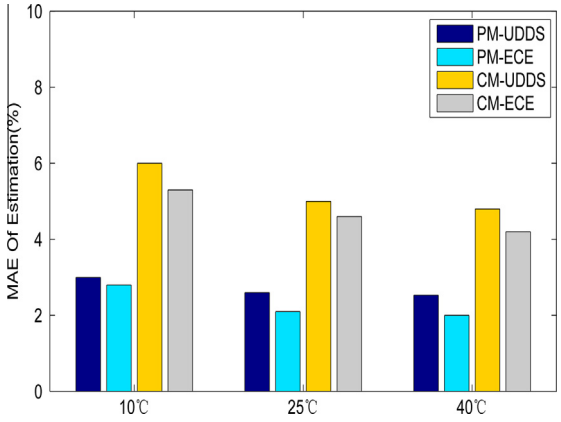

Fig. 11. The comparison of the MAE between UDDS operation and ECE operation for the battery (400 aging cycles).

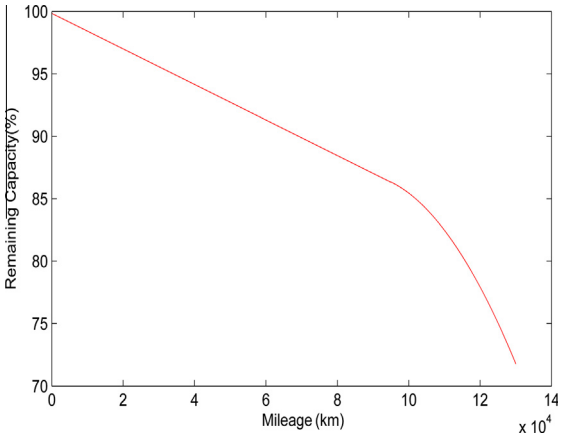

Fig. 12. The relationship between the practicable capacity of the Lithium Ion battery and the running mileage.

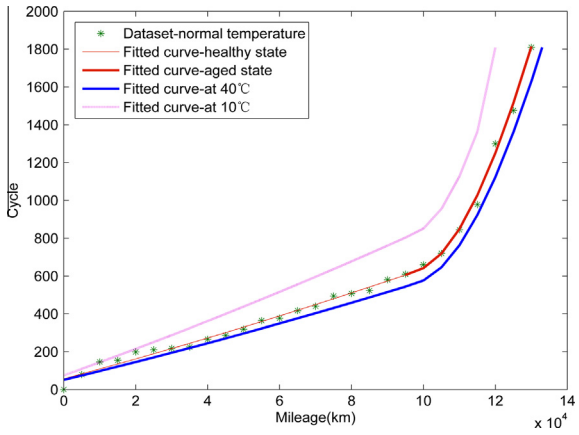

Fig. 13. The relation between the aging cycles and the running mileages of the Lithium Ion battery.

Table 2
The constants of the measurement equation of the 6Ah Lithium Ion battery.

Parameter	Mean value	Confidence (95%) internal
M	9.5×10^4	–
A	0.005680	[0.005289, 0.006071]
B	74.85	[54.25, 95.45]
C	9.278×10^{-7}	$[6.394 \times 10^{-7}, 1.216 \times 10^{-6}]$
D	−0.1746	[−0.2396, −0.1096]
E	8828	[5201, 12,460]

statistic analysis of the running mileage [16] and the running mileage of the battery is quite easy to get for electric vehicles. Based on the historical records of the SY6480A2-E electric vehicle using the 6Ah Lithium Ion batteries, the relationship between the practicable capacity and the running mileage for the Lithium Ion battery at normal temperature (10–40 °C) is showed in Fig. 12. Combined with the cycle life model of the battery, the relationship between the aging cycles of the battery and the running mileage can be ultimately built. As shown in Fig. 13, the aging cycles of the battery have a near linear relationship with the running mileage when the battery works in a healthy state. However, the aging cycles will increase significantly during the aged state of the battery. When the 6Ah Lithium Ion battery in the electric vehicle works at normal temperature, the measurement equation can be described as:

$$L_c = \begin{cases} Am + B & (m \leqslant M) \\ Cm^2 + Dm + E & (m > M) \end{cases} \quad (6)$$

where m is the running mileage of electric vehicle at normal temperature, L_c is the aging cycles of the battery, A, B, C, D and E are the constants determined by the data fitting. The fitting values of the constants at normal temperature are showed in Table 2.

6. Conclusions

The paper builds the cycle life model of the 6Ah Lithium Ion battery to predict the practicable capacity of the battery in the degradation process at different temperatures. The new model (PM) based on RBFNN and cycle life model is proposed to estimate SOC of the Lithium Ion battery. Numerical experiments and simulations with the UDDS and ECE datasets are presented to verify the accuracy of new model and the model's robustness against varying temperatures, aging cycles and loading profiles. It is significant to conclude that:

1. The practicable capacity of the Lithium Ion battery has a great regularity related to the aging cycles. The mathematical relationship between the practicable capacity and the aging cycles can be fitted as $C_n = ax^{0.5} + b$. The constant a and b are affected by the temperature.
2. PM has a good robustness against varying temperatures and the degradation of the battery. The MAE of SOC estimation for 6Ah Lithium Ion battery under different temperatures and aging cycles is below 5%.
3. PM has a good robustness against different loading profiles. Compared with UDDS operation, the maximum MAE of SOC estimation under ECE operation for the battery (400 aging cycles) reduces to 3%.
4. The aging cycles of the battery in electric vehicles can be measured indirectly with the running mileages of the battery in the electric vehicle.

Acknowledgements

This work was supported by the Science and Technology Research Project of Shaanxi Province (No. 2010K01-071). The help of Miss YeZhuo Li for proofreading the article is gratefully acknowledged.

References

[1] Ng KS, Moo CS, Chen YP, Hsieh YC. Enhanced coulomb counting method for estimating state-of-charge and state-of-health of lithium-ion batteries. Appl Energy 2009;86:1506–11.
[2] Piller S, Perrin M, Jossen A. Methods for state-of-charge determination and their applications. J Power Sources 2001;96:113–20.
[3] Pop V, Bergveld HJ, Notten P, Regtien PPL. State-of-the-art of battery state-of-charge determination. Meas Sci Technol 2005;16:93–110.
[4] Xing YJ, He W, Pecht M, Tsui KL. State of charge estimation of lithium-ion batteries using the open-circuit voltage at various ambient temperatures. Appl Energy 2014;113:106–15.
[5] Chiang YH, Sean WY, Ke JC. Online estimation of internal resistance and open-circuit voltage of lithium-ion batteries in electric vehicles. J Power Sources 2011;196:3921–32.
[6] Lee S, Kim J, Lee J, Cho BH. State-of-charge and capacity estimation of lithium-ion battery using a new open-circuit voltage versus state-of-charge. J Power Sources 2008;185:1367–73.
[7] Liaw BY, Jungst RG, Nagasubramanian G, Case HL, Doughty DH. Modeling capacity fade in lithium-ion cells. J Power Sources 2005;140:157–61.
[8] Hu X, Li S, Peng H. A comparative study of equivalent circuit models for Li-ion batteries. J Power Sources 2012;198:359–67.
[9] Moura S, Chaturvedi NA, Krstic M. Adaptive PDE Observer for Battery SOC/SOH Estimation. In: ASME 5th Dynamic systems and Control Conference; 2012. p. 101–110.
[10] Klein R, Chaturvedi NA, Christensen J, Ahmed J, Findeisen R, Kojic A. Electrochemical model based observer design for a lithium-ion battery. IEEE Trans Control Syst Technol 2010;19:654–63.
[11] Plett GL. LiPB dynamic cell models for kalman-filter SOC estimation. In: Proceeding of the 27th International Battery; 2002. p. 19–23.
[12] He H, Xiong R, Guo H. Online estimation of model parameters and state-of-charge of $LiFePO_4$ batteries in electric vehicles. Appl Energy 2012;89:413–20.
[13] Plett GL. Extended Kalman filtering for battery management systems of LiPB-based HEV battery packs. J Power Sources 2004;134:277–92.
[14] Xiong R, Sun FC, Chen Z, He HW. A data-driven multi-scale extended Kalman filtering based parameter and state estimation approach of lithium-ion polymer battery in electric vehicles. Appl Energy 2014;113:463–76.
[15] Charkhgard M, Farrokhi M. State-of-charge estimation for lithium-ion batteries using neural networks and EKF. IEEE Trans Ind Electron 2010;27:4178–87.
[16] He Y, Liu X, Zhang C, Chen Z. A new model for state-of-charge (SOC) estimation for high-power Li-ion batteries. Appl Energy 2013;101:808–14.
[17] Cheng B, Yanlu Z, Jiexin Z, Junping W, Binggng C. Ni-MH batteries state-of-charge prediction based on immune evolutionary network. Energy Convers Manag 2009;50:3078–86.
[18] Weigert T, Tian Q, Lian K. State-of-charge prediction of batteries and battery–supercapacitor hybrids using artificial neural networks. J Power Sources 2011;196:4061–6.
[19] Shen WX, Chan CC, Lo EWC, Chau KT. Adaptive neuro-fuzzy modeling of battery residual capacity for electric vehicles. IEEE Trans Ind Electron 2002;49:677–84.
[20] Cheng B, Zhifeng B, Binggang C. State of charge estimation based on evolutionary neural network. Energy Convers Manage 2008;49:2788–94.

[21] Shen Weixiang. State of available capacity estimation of lead-acid batteries in electric vehicles using neural network. Energy Convers Manage 2007;48:433–42.
[22] Morita Y, Yamamoto S, Lee SH, Mizuno N. On-line detection of state-of-charge in lead acid battery using radial basis function neural network. Asian J Control 2006;8:268–73.
[23] Jian W, Jiang X, Zhang J, Xiang Z, Jian Y. Comparison of SOC estimation performance with different training functions using neural network. In: 2012 14th international conference on modeling and simulation; 2012. p. 459–63.
[24] Zhihang C, Shiqi Q, Masrur MA, Murphey YL. Battery state of charge estimation based on a combined model of extended Kalman filter and neural networks. In: 2011 IEEE proceedings of international joint conference on neural networks; 2011. p. 2156–63.
[25] Alamgir M, Sastry AM. Efficient batteries for transportation applications. SAE paper (08CNVG-0036) 2008.
[26] Eddahech A, Briat O, Woirgard E, Vinassa JM. Remaining useful life prediction of lithium batteries in calendar ageing for automotive applications. Microelectron Reliab 2012;52:2438–42.
[27] National Development and Reform Commission, Lithium-ion traction battery for electric vehicles. Automotive Industry Standard of the People's Republic of China (QC/T 743-201X) 2012.
[28] Gui CQ. Influence of temperature on LiFePO4 Li-ion power battery. Battery Bimon 2011;41.
[29] Fang W, Bin F, Shiqiang L, Guogang Q, Xin H, Shuai H. Attenuation test and duplication of power battery's cycle life. J Automot Saf Energy 2012;3:71–6.